Structural basis of DNA binding to human YB-1 cold shock domain regulated by phosphorylation

Jingfeng Zhang [1],[†], Jing-Song Fan[2],[†], Shuangli Li[1], Yunhuang Yang[1], Peng Sun[1], Qinjun Zhu[1], Jiannan Wang[1], Bin Jiang[1], Daiwen Yang [2],[*] and Maili Liu[1],[*]

[1]State Key Laboratory of Magnetic Resonance and Atomic and Molecular Physics, Key Laboratory of Magnetic Resonance in Biological Systems, National Center for Magnetic Resonance in Wuhan, Innovation Academy for Precision Measurement Science and Technology, Chinese Academy of Sciences, Wuhan National Laboratory for Optoelectronics, Wuhan 430071, China and [2]Department of Biological Sciences, National University of Singapore, 14 Science Drive 4, 117543, Singapore

ABSTRACT

Human Y-box binding protein 1 (YB-1) is a multifunctional protein and overexpressed in many types of cancer. It specifically recognizes DNA/RNA through a cold shock domain (CSD) and regulates nucleic acid metabolism. The C-terminal extension of CSD and the phosphorylation of S102 are indispensable for YB-1 function. Until now, the roles of the C-terminal extension and phosphorylation in gene transcription and translation are still largely unknown. Here, we solved the structure of human YB-1 CSD with a C-terminal extension sequence (CSDex). The structure reveals that the extension interacts with several residues in the conventional CSD and adopts a rigid structure instead of being disordered. Either deletion of this extension or phosphorylation of S102 destabilizes the protein and results in partial unfolding. Structural characterization of CSDex in complex with a ssDNA heptamer shows that all the seven nucleotides are involved in DNA–protein interactions and the C-terminal extension provides a unique DNA binding site. Our DNA-binding study indicates that CSDex can recognize more DNA sequences than previously thought and the phosphorylation reduces its binding to ssDNA dramatically. Our results suggest that gene transcription and translation can be regulated by changing the affinity of CSDex binding to DNA and RNA through phosphorylation, respectively.

INTRODUCTION

Human Y-box binding protein 1 (YB-1) is a multifunctional protein regulating cell proliferation, embryonic development and stress response (1–3). It is overexpressed in many types of cancer and is classified as a proto-oncogene. It performs the functions through participating in DNA and RNA metabolism including DNA replication, DNA repair, transcription, pre-mRNA splicing, non-coding RNA biogenesis, stress granule and P-body formation (2,4–7). YB-1 can bind to DNA and RNA through specific and nonspecific ways (2). The specific binding is conferred by the cold shock domain (CSD) and nonspecific binding by basic regions at the C-terminal domain (CTD) of YB-1. A recent report has revealed that the arginine-rich region in the CTD is involved in interactions with RNA and ssDNA to form nucleoprotein filaments (8).

The canonical CSD of human YB-1 spans from the 51st to 129th residue (9). The boundary of CSD has been challenged as deletion of the C-terminal extension residues reduced the binding of chicken YB-2 to single-stranded DNA (ssDNA) (10,11). Previous studies have suggested that the flanking regions of CSD may also regulate nucleic acid binding (1). This indicates the extended terminal regions of CSD may be essential for efficient nucleic acid binding and proper folding of CSD.

YB-1 was initially found to specifically bind to a Y-box sequence (CCAAT/ATTGG, double stranded DNA (dsDNA)) located in the promoter of the major histocompatibility complex class II (12). Later, it was shown that YB-1 also can bind to other gene promoters which contain the Y-box sequence, such as epidermal growth factor receptor (EGFR) and multidrug resistance 1 (MDR1) (13,14). Using a generic oligonucleotide microchip, YB-1 was found to specially bind to sequences with CACC and CATC motifs for ssDNA and GGTG/CACC, GATG/CATC and

GTGG/CCAC for dsDNA ([15]). In addition, YB-1 can recognize CT rich sequences in MYC gene promoter ([16]). Because YB-1 does not recognize the 4-mer core sequence (ATTG and TTGG) of the Y-box efficiently ([15]) and there are some controversial reports about YB-1 regulating MDR1 gene through the Y-box sequence, it has been questioned whether the Y-box participates in the binding ([17]).

Similar to ssDNA, RNA CACC and CAUC motifs have high affinity to YB-1, but CUGC, CA and CG repeats have low affinity ([18]). Investigation of YB-1 targets shows other RNA motifs exist too. YB-1 binds to 3′-UTR (untranslated region) of its own mRNA through 5′-UCCAGCAA-3′ and 5′-UCCAACAA-3′, which contain CAGC and CAAC motifs ([19]). In CD44 exon v4, YB-1 binds to the consensus sequence CAACCACA ([20]), which contains CAAC and CCAC motifs. Clearly, the DNA and RNA motifs to which YB-1 binds share similar sequences as nucleic acid bases contribute mostly to the interactions with YB-1 ([21]).

YB-1 CSD contributes to specific recognitions of DNA and RNA, but most of the studies have focused on the full-length YB-1. There is lack of information about how the isolated CSD interacts with different nucleic acid sequences.

Two crystal structures of YB-1 CSD in complex with RNAs were reported in 2019 ([21],[22]). The structures show that four RNA bases CAUC/CACC bind to CSD through two nucleic acid binding motifs: RNP1 and RNP2. On the basis of the structures, the C-terminal extension seems to have no contribution to RNA binding, contradictory to the previous results ([10],[11]). Therefore, it is necessary to further characterize the structural role of the C-terminal extension in interactions with nucleic acids.

Posttranslational modification plays an important role in regulating the function of YB-1. S102 located at YB1 CSD can be phosphorylated by RSK1/2 and AKT ([23]). In tumors from cancer patients, YB-1 is highly phosphorylated ([24]). Anticancer reagents, ionizing radiation, UV exposure and growth factors also can induce YB-1 phosphorylation ([23–26]). It has been shown that the phosphorylation of S102 affects both DNA transcription and RNA translation ([14],[27–30]). According to the current structural information, however, S102 is not involved in nucleic acid binding ([21]). How phosphorylation of this amino acid regulates gene transcription and translation through nucleic acid binding needs further structural study.

Here, we reported the solution structures of human YB-1 CSD with a C-terminal extension of 11 amino acids in ssDNA-free and -bound forms using NMR spectroscopy. The structures suggest that the C-terminal extension plays a critical role in stabilizing the structure of CSD and participates in direct interactions with ssDNA. We further showed that phosphorylation of S102 results in local unfolding of the CSD due to the destabilization effect and reduces significantly ssDNA binding affinity.

MATERIALS AND METHODS

Purification of YB-1 CSD and CSDex

YB-1 CSD (D51-G129) and CSDex (D51-A140) were cloned into a modified pET32a vector with an N-terminal His-tag. The protein was expressed using BL21(DE3) bacterial strain in LB or M9 medium supplemented with ^{15}N

NH_4Cl or both ^{15}N NH_4Cl and ^{13}C-labeled glucose and the overexpression was induced with 0.1 mM IPTG at 20°C overnight. The protein was purified using a Ni-NTA agarose column and the His-tag was removed by thrombin. The large molecular weight aggregate was removed by passing the protein solution through a HiLoad 16/600 Superdex 75 pg column (GE healthcare) in a buffer containing 20 mM sodium phosphate (pH 7.4), 300 mM NaCl and 1 mM EDTA. The purified protein was confirmed to be nucleic acid free by measuring the ratio of OD_{260}/OD_{280} to be <0.65. The single point mutants S102A, S102D and S102E were purified using the same procedure.

YB-1 CSD phosphorylation

Human active RSK1 (R1031) was purchased from Sigma Aldrich. CSDex was phosphorylated by RSK1 following the procedure provided by the manufacturer with minor changes. Briefly, purified ^{15}N-labeled CSDex was changed into a buffer containing 5 mM MOPS (pH 7.2), 50 mM NaCl, 2.5 mM β-glycerolphosphate, 5 mM $MgCl_2$, 1 mM EGTA, 0.4 mM EDTA, 5 mM DTT and 1 mM ATP. RSK1 was added into the protein solution to catalyze the reaction at 30°C overnight. The phosphorylation was examined by mass spectrometry (MS) (Agilent Technologies 6530 Accurate-Mass Q-TOF LC/MS) in the electrospray ionization mode. The phosphorylated CSDex (^{P}S102) was changed into buffer A (20 mM sodium phosphate (pH 7.4), 50 mM NaCl and 1 mM EDTA) and adjusted to 0.1 mM protein for recording NMR ^{1}H–^{15}N HSQC.

NMR spectroscopy and structure calculation

NMR experiments were performed on DNA-free and DNA-bound samples at 298 K using an 800 MHz Bruker AVANCE NMR spectrometer equipped with a 5-mm cryogenic probe. The DNA-free sample contained 0.8 mM ^{13}C,^{15}N-labeled CSDex in a 20 mM sodium phosphate buffer (pH 7.4), 50 mM NaCl, 1 mM deuterated EDTA (d_{16}) and 3% D_2O. The DNA-bound sample contained 1.0 mM ^{13}C,^{15}N-labeled CSDex and 1.0 mM ssDNA (5′-AACACCT-3′) in the same buffer as that for the DNA-free sample. 2D HSQC, 3D HNCA, HNCOCA and MQ-(H)CCH-TOCSY ([31]), and 4D NOESY ([32]) were recorded to obtain backbone and sidechain resonance assignments. ^{1}H chemical shift assignments of the ssDNA were achieved using 2D ^{13}C/^{15}N-filtered TOCSY and NOESY ([33]). NMR spectra were processed using NMRPipe ([34]) and analyzed using NMRFAM-Sparky ([35]). Backbone and sidechain resonance assignments were achieved using the NOESY-based strategy ([36],[37]). Unambiguous intra-molecular NOEs were obtained from three sub-spectra: ^{13}C,^{15}N-edited, ^{13}C,^{13}C-edited and ^{15}N,^{15}N-edited 4D NOESY. Inter-molecular NOEs between CSDex and ssDNA were identified from a 3D ^{13}C,^{15}N-filtered/edited NOESY experiment ([38]). Distance constraints obtained from the assigned NOEs were divided into three classes based on the intensities of NOE cross-peaks: (i) strong: 1.8 Å < d < 2.9 Å, (ii) medium: 1.8 Å< d < 3.5 Å and (iii) weak: 1.8 Å < d < 5 Å, while the dihedral angle restraints of φ and ψ were calculated with TALOS+ using the assigned chemical shifts of C_α, C_β,

N, H_α and H_N (39). The solution structure was calculated with Xplor-NIH (40,41) using the torsion angle molecular dynamics protocol. The refinements for ssDNA-free and -bound structures were performed using RNA ff1 (42) and eeFX force-fields (43), respectively. 20 conformers from a total of 100 calculated ensembles with the lowest energy were selected for analysis.

Steady-state $^{15}N–\{^1H\}$ heteronuclear NOE values of CS-Dex were measured on a 700 MHz spectrometer at 298 K according to the previously described method (44). In the measurements, the recycle delay was 8 s and the proton saturation time was 4 s. The $^{15}N–\{^1H\}$ NOE values were derived from ratios of the peak intensities with and without proton saturation.

2 mM ssDNA (5′-CAACACCT-3′) was titrated into 0.1 mM ^{15}N-labeled CSDex solution and $^1H–^{15}N$ HSQC spectra at a series of ssDNA concentrations were acquired on a 600 MHz Bruker AVANCE II spectrometer.

Measurement of affinity of ssDNA binding to protein by ITC

Purified CSDex, its mutants, and phosphorylated CSDex each were prepared in buffer A at 10 μM. All the ssDNAs were purchased from Tianyi Huiyuan Biotech Co. and dissolved in buffer A at 100 μM. To obtain affinities of ssDNAs binding to CSDex, its mutants, and phosphorylated CSDex, isothermal titration calorimetry (ITC) was performed at 298 K on a VP-ITC instrument (GE Healthcare).

Determination of apparent molecular weight of YB-1 CSDex by gel filtration

YB-1 CSDex was passed through a HiLoad 16/600 Superdex 75 pg column (GE healthcare) in a buffer containing 20 mM sodium phosphate (pH 7.4), 300 mM NaCl and 1 mM EDTA. The CSDex concentration of the loaded sample was 10 mg/ml. The elution volumes of standards were used to estimate the molecular weight of CSDex in aqueous solution.

RESULTS

C-terminal extension of CSD stabilizes the folded structure

Human YB-1 CSD with the conventional domain boundary (D51-G129) exhibited two sets of $^1H–^{15}N$ correlations (Figure 1A). One set is characteristic of disordered (unfolded) proteins with ^1H chemical shifts in a narrow range of ∼7.9–8.5 ppm, while the other is characteristic of folded proteins. This is consistent with the previous study (45). The result shows that this CSD construct exists in two conformations, one folded and one unfolded or disordered, which undergo slow conformational exchange in the NMR time regime. The result also implies that this CSD is marginally stable and can unfold easily. To clarify how the residues close to the termini affect CSD stability, a number of constructs with different sequence lengths were tested. In the end, the shortest stable construct was identified to consist of 90 residues from D51 to A140, which is denoted as CSDex. The $^1H–^{15}N$ HSQC spectrum of CSDex showed one set of signals, indicating that the protein exists in a single folded

form (Figure 1B) and also implying that CSDex is more stable than the CSD construct**.** CSDex eluted at ∼90 ml on a size exclusion column pg75 16/600 (Supplementary Figure S1), between the standard Aprotinin (∼95 ml, 6.5 kDa) and Ribonuclease A (∼80 ml, 13.7 kDa), indicating that it exists as a monomeric form (∼10 kDa) even at a concentration of 10 mg/ml.

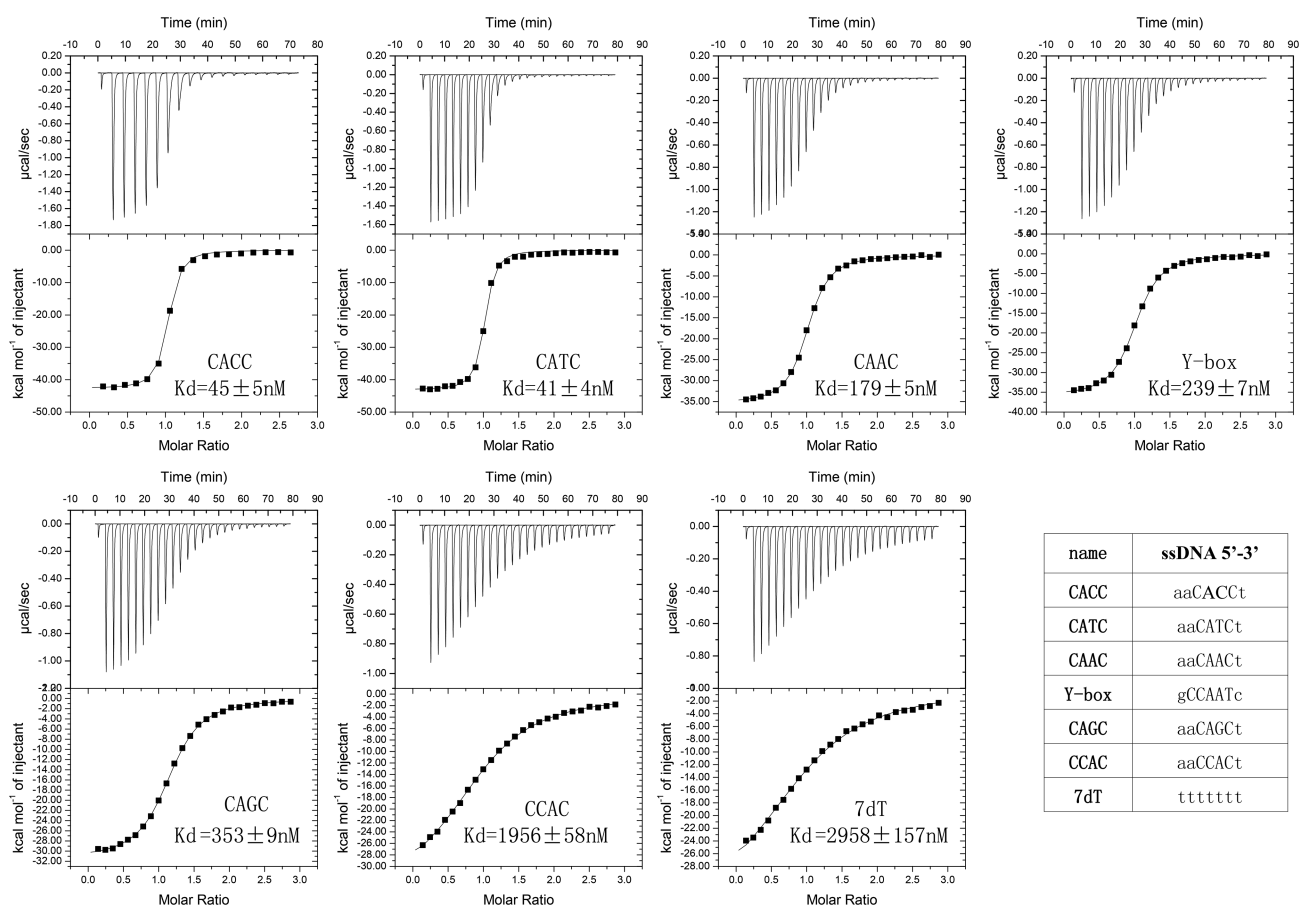### YB-1 CSDex exists as a compact folded structure

Using triple-resonance NMR experiments, we obtained backbone and sidechain resonance assignments. Apart from proline, four residues (V68, N94, Y99 and E117) were not assigned in backbone resonances because their $^1H–^{15}N$ correlations were missing in the HSQC. In the previous study on YB-1 CSD without the C-terminal extension, fourteen non-proline residues (K64, W65, N67, V68, Y72, K93-N95, R97-Y99 and R101-V103) were not observed in the $^1H–^{15}N$ HSQC due to conformational exchanges in the intermediate exchange regime (9). Here, 89% (481/540) of proton resonances were assigned for CSDex, which ensures to obtain a sufficient number of $^1H–^1H$ NOE assignments. Using distance restraints derived from the assigned $^1H–^1H$ NOEs and dihedral angle restraints derived from the chemical shifts (Supplementary Table S1), the structure of CSDex was determined. The NMR assignments and 20 solution structure models have been deposited in BMRB (ID: 36307) and PDB (ID: 6LMS), respectively. Overall, CSDex adopts a barrel structure with five antiparallel β-strands: β1 (K53-N67), β2 (G71-R77), β3 (K81-H87), β4 (G106-G116) and β5 (A120-A123) (Figure 2). The loops connecting the strands (loop12, loop23, loop34 and loop45) are slightly less converged than the β-strands and have fixed orientations with respect to the barrel. $^{15}N–\{^1H\}$ heteronuclear NOE data (Supplementary Figure S2A) also support that the loops are relatively rigid and just slightly more flexible than the β-strands. Although the C-terminal extension (G130-A140) does not adopt a regular secondary structure, it exists as a well-defined long loop with extensive interactions with loop12 and loop34. For instance, following inter-residue $^1H–^1H$ NOEs were observed: Y138 – V68, G135–V103, G135–G104 and S136–S102. The $^{15}N–\{^1H\}$ heteronuclear NOE values for this loop are similar to those for the β-strands (Supplementary Figure S2A), further demonstrating that the C-terminal extension is rigid rather than flexible and disordered. For the CSD without the extension, most residues in loop34 (K93–Y99, R101–V103) had very weak or invisible $^1H–^{15}N$ correlations (Figure 1A) (9,45), suggesting that this region undergoes conformational exchanges on ms-μs timescales. For CSDex, however, only N94 and Y99 in this loop were invisible in the HSQC. This result shows that the mobility of loop34 on ms-μs timescales is also reduced significantly by the C-terminal 11-residue extension. Structural comparison shows that the overall β-barrel structure of CSDex is similar to the CSD structure (PDB ID: 1H95) solved previously (9,45), but loop34 is defined much better in CSDex than in CSD (Figure 2A), resulting from extra interactions of this loop with the C-terminal extension. The chemical shifts of amides located in the regular β-strands of CSDex and CSD are simi-
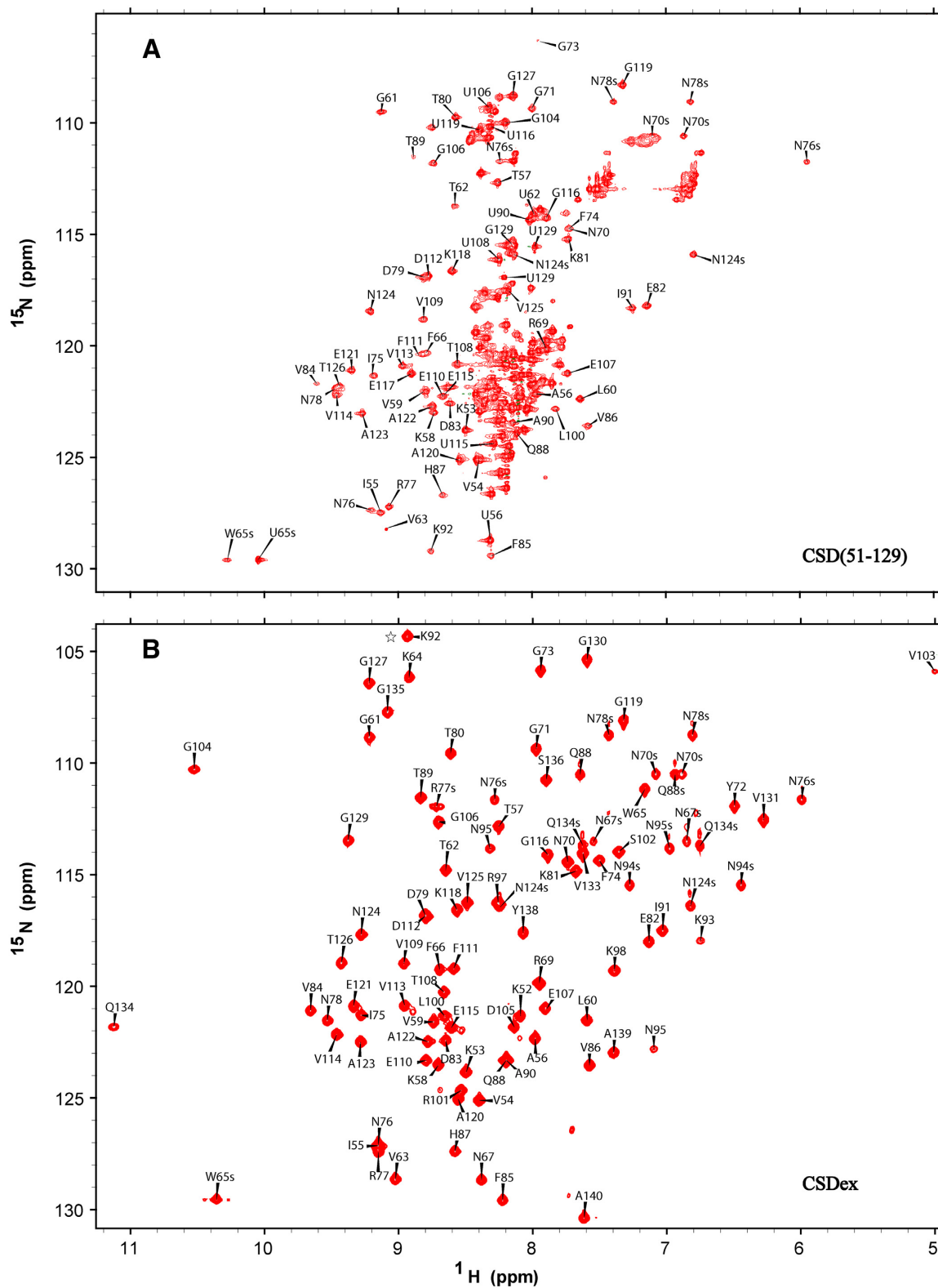
Figure 1. ^1H–^{15}N HSQC spectra of CSD (**A**) and CSDex (**B**). Peak assignments of CSDex are labeled. For CSD (aa 51–129), the assignments were retrieved from the published data ([45]) and the residues from the unfolded form are indicated by appending 'U' in front of residue numbers. The peaks from the sidechains of W, Q and N are labeled by appending "s" after the residue numbers.
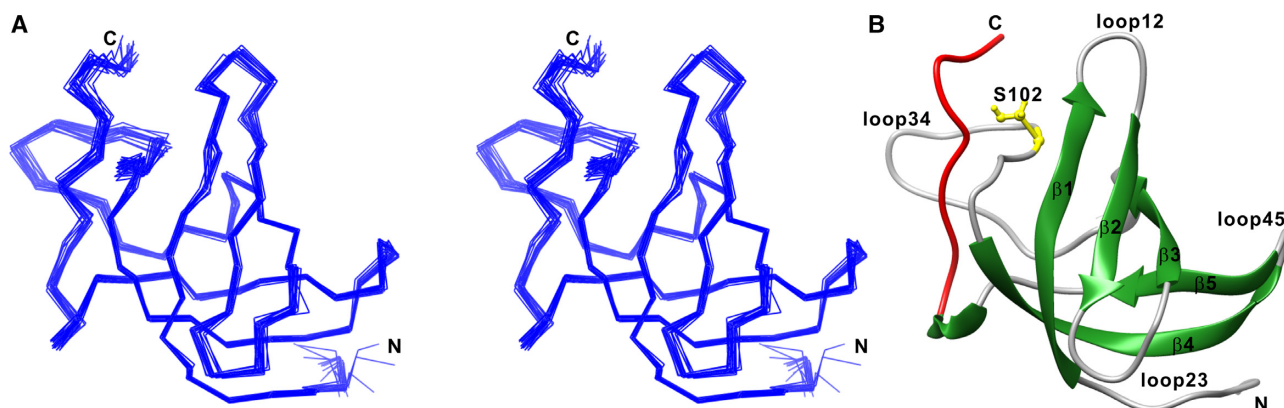
Figure 2. (**A**) Stereo view of an ensemble of twenty structures of CSDex superimposed for residues 53–67, 72–77, 83–88, 108–116, 119–126 and 130–139. (**B**). Ribbon diagram of the lowest energy structure of CSDex. The five β-strands are shown in green. The C-terminal extension from G130 to A140 is highlighted in red and the side-chain of residue S102 is shown in yellow. The four loop regions (loop12, loop23, loop34 and loop 45) are colored in gray.

name	ssDNA 5'-3'
CACC	aaCACCt
CATC	aaCATCt
CAAC	aaCAACt
Y–box	gCCAATc
CAGC	aaCAGCt
CCAC	aaCCACt
7dT	ttttttt

Figure 3. ITC profiles of CSDex binding to a series of ssDNAs. The experimental data are indicated by dots. The solid lines are the best fits. K_d values extracted from data fitting are given in the plots. The stoichiometric binding ratios obtained for all the DNAs are close to 1.

lar, but the amide chemical shifts in loop34 are very different (Supplementary Figure S3), consistent with the conclusion drawn from the structural comparison.

ssDNA binds to CSDex in a sequence-specific way

To examine the binding affinities of CSDex to different ssD-NAs, we performed ITC experiments. All the ssDNAs used here are identical in sequence length (Figure 3). The ITC profiles and extracted K_d values are summarized in Figure 3. The CCAC motif and 7dT bound to CSDex in μM affinity, indicating non-specific binding. Other motifs had much higher affinities, suggesting that the binding of CSDex to ss-DNA is sequence specific. The binding affinity from higher to lower is in the order of CATC > CACC > CAAC > Y-box (CAAT) > CAGC > CCAC > 7dT.
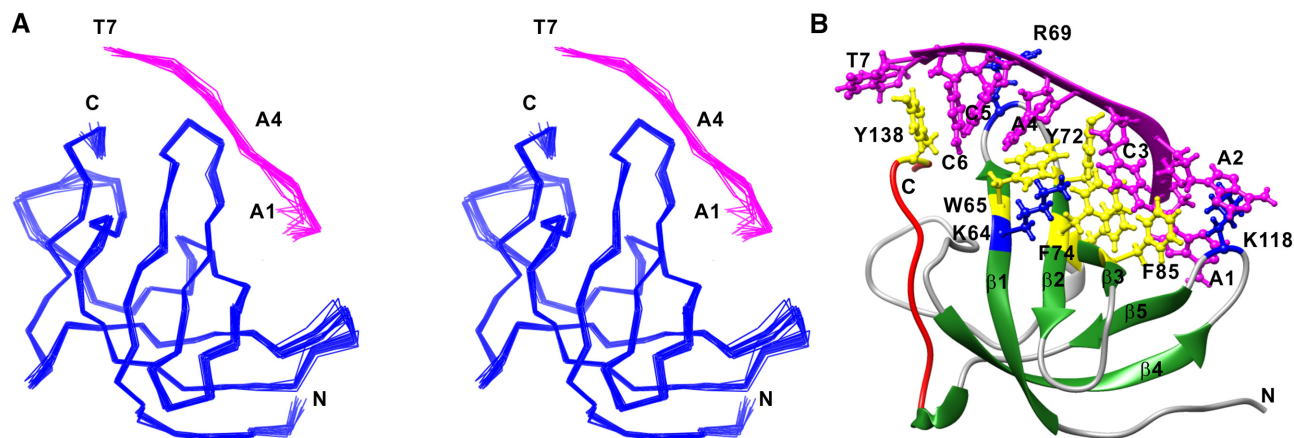
Figure 4. (**A**) Stereo view of an ensemble of twenty structures of CSDex (blue) in complex with a ssDNA (5′-AACACCT-3′) (magenta) superimposed for residues 53–67, 72–77, 83–88, 108–116, 119–126 and 130–139. (**B**) Ribbon diagram of the lowest energy structure of CSDex-ssDNA complex. The five β-strands are shown in green. The C-terminal extension from G130 to A140 is highlighted in red. The bases are represented by sticks and balls in purple. The residues involved in interactions with ssDNA are shown by sticks and balls in yellow (W65, F74, F85, H87 and Y138) and blue (K64, R69 and K118).

Structure of CSDex–ssDNA complex

To better understand how CSDex interacts with ssDNA, we solved the structure of CSDex in complex with an ssDNA heptamer (5′-AACACCT-3′) using NMR. In the presence of the heptamer, only one non-proline residue (R101) was not assigned in backbone resonances. Using intra- and inter-molecular ^1H–^1H distance and dihedral angle restraints derived from NMR experiments (Supplementary Table S1), the structure was determined. The NMR assignments and 20 structure models have been deposited in BMRB (ID: 36306) and PDB (ID: 6LMR), respectively. The overall structure of CSDex in the ssDNA-bound form is similar to that in the ssDNA-free form (Figures 4 and 2). Interestingly, all loops in the DNA-bound form are converged better than those in the DNA-free form (Figures 2 and 4). The ^{15}N–$\{^1H\}$ heteronuclear NOE data (Supplementary Figure S2B) also indicate that the loops become more rigid upon binding to the ssDNA. The ssDNA adopts an arc shape and binds onto the surface formed by β1 to β3. From the complex structure, it is clearly shown that all the seven DNA nucleotides are involved in binding to the protein. Intermolecular NOEs between residues H87, F85, F74, Y72, N70, N67 and W65 to nucleotides were observed in the CSDex/ssDNA complex (Supplementary Table S2, Figure S4). In addition, π–π stacking interactions between Y138 in the C-terminal extension and C6 are found in the complex (Supplementary Figure S4, Table S2). Besides aromatic residues, several positive charged residues such as K64, R69 and K118 may contribute to DNA binding through charge-charge interactions (Supplementary Table S2). Apart from the previously identified three nucleic acid binding regions: RNP1 (W65-N70 and Y72-F74), RNP2 (F85, H87) and loop45 (K118) (21,22), we found one extra region locating at the C terminal extension (Y138) (Figure 4).

Phosphorylation of S102 destabilizes CSDex and reduces DNA binding affinity

CSDex was phosphorylated with RSK1, and the phosphorylation was confirmed by MS. The measured molecular weight of CSDex before phosphorylation was 9927.3 Da, which is close to the predicted molecular weight 9927.1 Da (Supplementary Figure S5A). After phosphorylation reaction, the molecular weight changed to 10007.3 Da, showing that the protein was phosphorylated successfully (Supplementary Figure S5B). According to the intensities of two sets of MS peaks from the phosphorylated and non-phosphorylated forms, ~95% CSDex was phosphorylated (Supplementary Figure S5B).

After phosphorylation, several backbone ^1H–^{15}N correlations disappeared or shifted too far away from the original positions, including K92, K98, S102, V103, G104, Q134, G135 and S136 (Figure 5). These residues perturbed by the phosphorylation are located at loop34 and C-terminal extension, which are spatially close to the phosphorylation site S102 (Figure 2). In addition, the sidechain NH group of W65 displayed two ^1H–^{15}N NMR correlations: one corresponding to the folded form and the other to the unfolded form. Moreover, some extra ^1H–^{15}N correlations appeared in the region of 7.9–8.5 ppm on the ^1H dimension (Figure 5). This spectral feature is similar to that for the CSD lack of the C-terminal extension, suggesting that the phosphorylated CSDex exists in two forms: one being folded, and the other being locally unfolded or fully unfolded. Three very resolved peaks at ~8.35 ppm for ^1H and ~110 ppm for ^{15}N were assigned to G106, G116 and G119 in the unfolded form by comparing ^1H–^{15}N chemical shifts of $^PS102$ and CSD (Figures 1A and 5). According to signal intensity ratios of the folded and unfolded correlations, the populations of individual residues in the unfolded form were estimated to be 25% for W65 sidechain, 20% for G106, 6% for G116, and 4% for G119. The population variation among different residues suggests that locally unfolded forms instead of a fully unfolded form exist in the phosphorylated sample. Taken together, phosphorylation disrupts the interactions of S102 with its surrounding residues and destabilizes the folded structure, in turn shifts the dynamic folded-unfolded equilibrium towards the locally unfolded form.

To determine the effect of the phosphorylation on DNA binding, we performed ^1H–^{15}N HSQC titration using a ss-DNA (5′-AACACCT-3′). For non-phosphorylated CSDex,
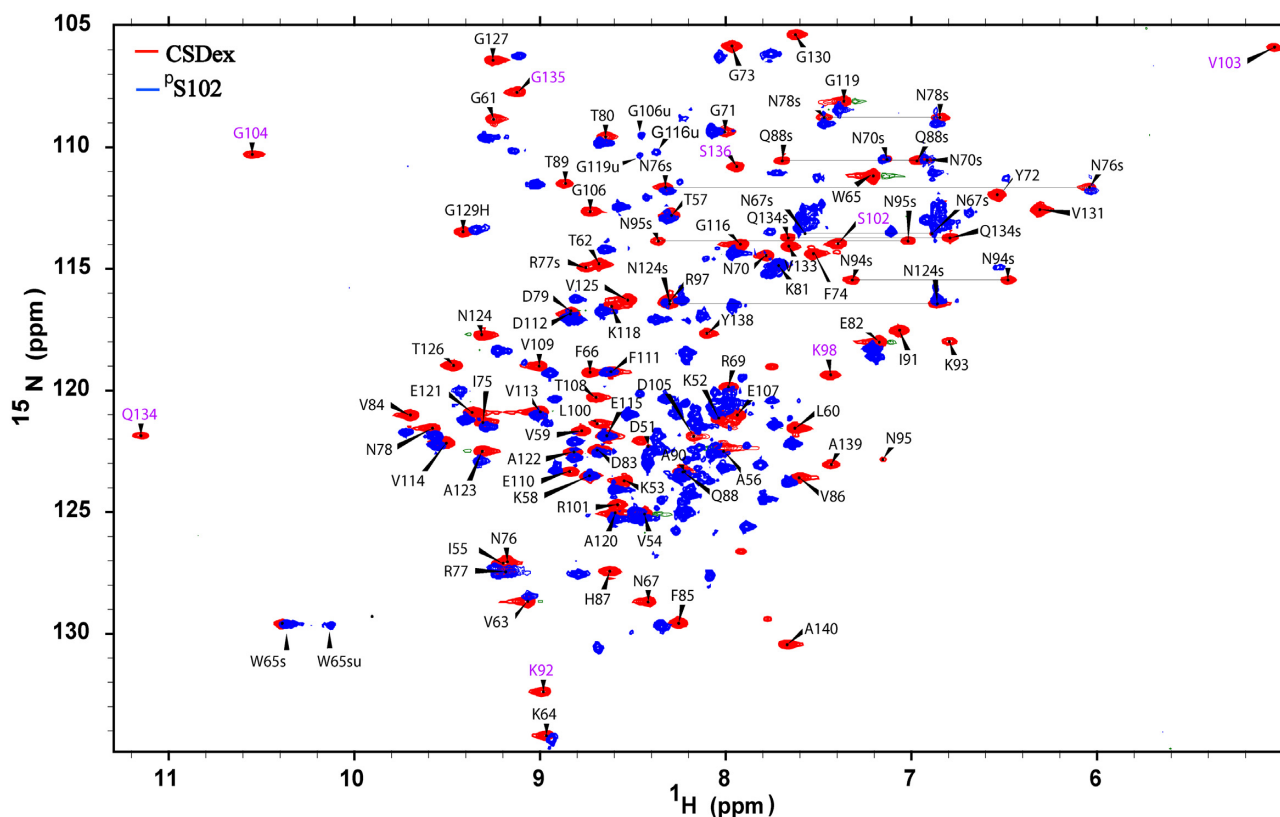
Figure 5. ^{1}H–^{15}N HSQC spectra of CSDex (red) and phosphorylated CSDex (^{P}S102, blue). Peak assignments of CSDex are labeled. The peaks that disappeared or shifted too far away from the original positions after phosphorylation are labeled in purple. For ^{P}S102, the peaks of W65 sidechain in the folded and unfolded forms are labeled as W65s and W65su, respectively, while the peaks of G106, G116 and G119 in the unfolded form of ^{P}S102 are labeled as G106u, G116u and G119u.

the original set of peaks gradually decreased in intensity, a new set of peaks appeared and increased in intensity, and the peak positions did not change with the increase of DNA concentration during the titration (Supplementary Figure S6A). This indicates that the DNA-bound and DNA-free forms are in slow exchange in the NMR time regime and the binding is strong, consistent with the ITC result. For phosphorylated CSDex, in contrast, the original set of peaks shifted gradually in position with the increase of DNA concentration (Supplementary Figure S6B), indicating that the DNA-bound and DNA-free forms are in fast exchange and the binding is weak. According to our ITC data (Figure 6), the affinity of ^{P}S012 to a ssDNA (9.4 μM) was about 200 times lower than that of WT CSDex to the same ssDNA (45 nM). Since the phosphorylation at S102 disturbs the structures of two DNA-binding regions (one around W65 and the other in C-terminal extension), it is not surprised that the phosphorylation reduces the ssDNA binding affinity. The results demonstrate the importance of S102 for the stability of CSDex and its binding affinity to ssDNA.

To further understand the importance of S102 to DNA binding, we mutated S102 to D and E separately to mimic the phosphorylated protein. The ^{1}H–^{15}N HSQC spectra of S102D and S102E mutants displayed the characteristic peaks from the unfolded form, including the W65 sidechain peak and G106, G116 and G119 amide peaks (Supple-

mentary Figure S7). On the basis of the peak intensity ratios, the unfolded populations of S102E were 21% for W65 sidechain, 9% for G106, 4% for G116, and 2% for G119; while the unfolded populations of S102D were 11% for W65 sidechain, 7% for G106, 3% for G116 and 1% for G119. The spectral features for S102D, S102E and ^{P}S102 are similar although the unfolded populations are not the same. The results indicate that S102D and S102E can mimic ^{P}S102.

Based on ITC experiments, the binding affinities of S102D and S102E to ssDNA (5′-AACACCT-3′) were 1.8 and 4.0 μM respectively (Figure 6), which are at the same order as that of ^{P}S102, but are more than 40 times lower than that of WT CSDex (45 nM). To assess if the affinity change is caused simply by point mutation or phosphomimetic effect, S102A was generated. This mutant gave rise to a similar spectral pattern to S102D and S102E (Supplementary Figure S7). The unfolded populations were about 17% for W65 sidechain, 6% for G106, 4% for G116 and 1% for G119. Its affinity to the ssDNA was ∼0.6 μM (Figure 6), much lower than that for WT CSDex but significantly higher than those for S102D and S102E. The results further support that S102 is essential to the stability of CSDex and the binding affinity to ssDNA. Replacement of the hydroxyl group at S102 sidechain by mutation or phosphorylation will destabilize CSDex and reduce its affinity to ssDNA.
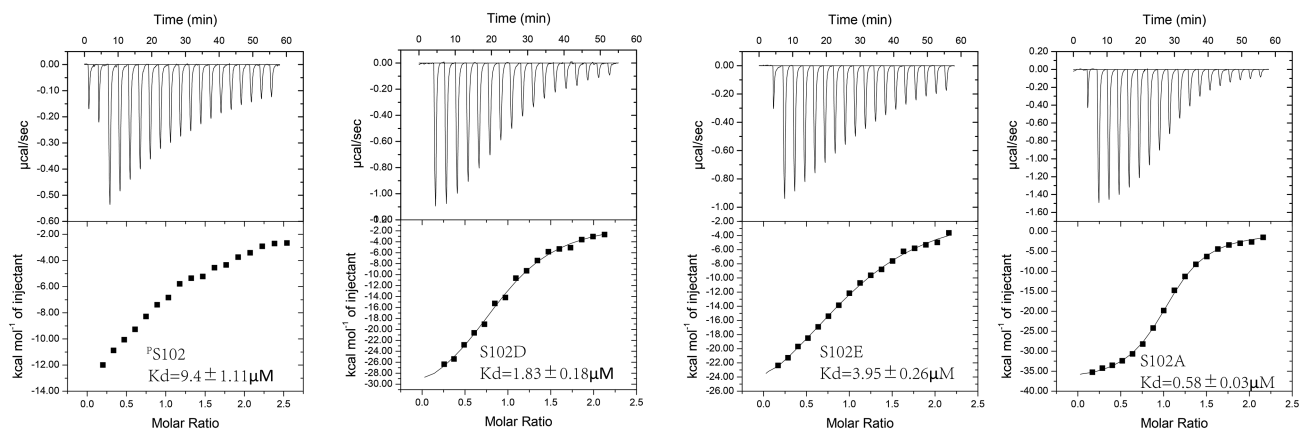
Figure 6. ITC profiles of phosphorylated CSDex ($^{\mathrm{P}}$S102), CSDex mutants S102D, S102E and S102A binding to ssDNA (5′-AACACCT-3′).

DISCUSSION

It has long been reported that human YB-1 CSD exists in a dynamic equilibrium between folded and unfolded forms (9,45). According to our result, the CSD with an 11-residue C-terminal extension exists in a well folded form. The unfolded form observed for the conventional YB-1 CSD is simply caused by inappropriate selection of the domain boundary. Thus, the cold shock domain in the full-length YB-1 should adopt a folded stable structure and the interactions of the 11-residue extension (GVPVQGSKYAAD) with loop34 and loop12 should be independent of the sequence beyond A140. The C-terminal extension sequence, which is in interactions with the phosphorylation site S102 as well as ssDNA, is quite conserved in YB-1 from different species (Figure 7), demonstrating its importance. Besides YB-1, other CSD-containing proteins such as Lin28, CRHSP24 and UNR from eukaryote also contain C-terminal extension sequences (46–49) although the extension sequences have low similarity between different types of proteins (Figure 7). On the other hand, the CSD-containing proteins from bacteria are lack of the extension sequence (50). This implicates that the extended C-terminal sequences are structural and functional important only for eukaryotic CSD-containing proteins.

Very recently, two YB-1 CSD/RNA complex structures have been solved by X-ray crystallography. In one structure the CSD from human consists of 81 residues (G50–G130) without the C-terminal extension. In the other structure, the CSD from zebrafish consists of 93 residues with the C-terminal extension (D30-R122, corresponding to human YB-1 D51-R142), and this extension adopts a loop structure, similar to that obtained in this study. Note that the CSDex domains from human and zebrafish are identical in amino acid sequences. In both the X-ray structures, the RNAs used consist of six nucleotides and only four core nucleotides are involved in interactions with two common binding regions in CSD: RNP1 (W65, F74) and RNP2 (F85, H87). In the structure of the CSD from zebrafish, one of the four core nucleotides also interact with loop45. Although the protein in our CSDex/ssDNA complex adopts a structure similar to the zebrafish CSD, all the seven nucleotides in our heptamer ssDNA instead of four are in contacts with CSDex. Besides the RNP1, RNP2 and loop45, the C-terminal extension (Y138) interacts with Cyt6 and Thy7 in the ssDNA most likely through π–π interactions. Our structure explains the previously reported data that deletion of the C-terminal region of chicken YB-2 CSD results in the loss of its ssDNA binding (10,11). According to our structure, apart from the four core nucleotides, the flanking sequence is important for proper DNA/RNA binding, supporting the previous suggestion that efficient binding of YB-1 to RNA may require an appropriate flanking RNA sequence (18).

Although Y138 has interactions with Cyt6 and Thy7 in our CSDex–DNA complex, the DNA binding does not induce a significant structural change of the region G130–A140. In the work by Kretov *et al.* (8), G130–140 was assumed to adopt a random coil structure and Y138 was considered to have no interactions with any nucleotides. Using PRE (paramagnetic relaxation enhancement) experiment, Kretov *et al.* found that the distances between the amides of G135, S136 and K137 and the sidechain of T62 are shorter in the DNA-free form than in the 10 nt ssDNA-bound form. The distance change information was derived from NMR peak intensity difference, but the exact distance change was not calculated. Because PRE is inversely proportional to the sixth power of the distance between a nuclear spin and a free radical (located at the MTSL), 10% change of a distance from 15.0 to 16.5 Å will result in ∼60% reduction of the PRE. In addition, the distance change can be caused by altering backbone or/and sidechain conformations. Therefore, the structural change induced by DNA binding should not be significant for CSDex.

Similar to YB-1, the CSDs in Lin28 and UNR from eukaryotic organisms also use RNP1, RNP2 and loop45 as ssDNA and RNA binding sites (47,48,51). Sequence comparison shows that loop45 and its adjacent residues are partially conserved with one invariable positively charged residue (Figure 7), suggesting that CSDs from different eukaryotic species may bind to nucleic acids through three common binding sites: RNP1, RNP2 and loop45. On the other hand, the binding site located in the C-terminal extension is likely unique to YB-1 since the homology of the extension sequences from different family proteins is low (Figure 7).

```
                45                      RNP1                    RNP2               106
YB1_HS      AAPA-GGDKKVIATKVLGTVKWFNVRNGYGFINR--------N-DTKEDVFVHQTAIKKNNPRKYLRSVGDG
YB1_DR      AAAT-AGDKKVIATKVLGTVKWFNVRNGYGFINR--------N-DTKEDVFVHQTAIKKNNPRKYLRSVGDG
YB1_DS      GKLV-QPPKELIATKVTGTVKWFNVKSGYGFINR--------N-DTKEDVFVHQSAIARNNPKKAVRSVGDG
LIN28_HS    GKLPEPAEEESQVLRGTGHCKWFNVRMGFGFISMINREGSPL-DIPVDVFVHQSKLFMEG----FRSLKEG
CSPA_EC     -----------MSGKMTGIVKWFNADKGFGFITP-------D-DGSKDVFVHFSAIQNDG----YKSLDEG
CRHSP_HS    TRTFSATVRASQGPVYKGVCKCFCRSKGHGFITP--------A-DGGPDIFLHISDVEGEY----V--PVEG
UNR_CSD1_DM SNSSAAAADPSQTTRETGI--IEKLLHSYGFIQCC--------ERQARLFFHFSQFSGNI-----DHLKIG
UNR_CSD1_HS -GHNGYPNGTSAALRETGVIE--KLLTSYGFIQC--------S-ERQARLFFHCSQYNGN-----LQDLKVG
UNR_CSD2_HS VSARNIMLLKKKQARCQGVVC--AMKEAFGFIER--------G-DVVKEIFFHYSEFKGD-----LETLQPG
UNR_CSD3_HS IEVLSNTFQFTNEAREMGVIA--AMRDGFGFIKC--------V-DRDVRMFFHFSEILDG------NQLHIA
UNR_CSD4_HS ATCVRLLGRNSNSKRLLGYVA--TLKDNFGFIET--------A-NHDKEIFFHYSEFSGD-----VDSLELG
UNR_CSD5_HS LGQNAQTMAYNITPLRRATVE--CVKDQFGFINY--------EVGDSKKLFFHVKEVQDG------IELQAG
                          .                  .***               :*.*.                .
                107         loop45              144
YB1_HS      ETVEFDV----VEGEKGAEAANVTGPGGVPVQGSKYAADRNH
YB1_DR      ETVEFDV----VEGEKGAEAANVTGPGGVPVQGSKYAADRNR
YB1_DS      ELVEFDV----VIGEKGNEAANVTGPSGEPVRGSQFAADKRR
LIN28_HS    EPVEFTF----KKSSKGLESIRVTGPGGSPCLGSERRPKGKT
CSPA_EC     QKVSFTI----ESGAKGPAAGNVTSL----------------
CRHSP_HS    DEVTYKM---CSIPPKNEKLQAVEVVITHLAPGTKHETWSGH
UNR_CSD1_DM DPVEFEMTYDRRT-GKPIASQVSKIAPEVVLSEERVTGTVTT
UNR_CSD1_HS DDVEFEV----SSDRRTGKPIAVKLVKIKQEILPEERMNGQE
UNR_CSD2_HS DDVEFTI---KDRNGKEVATD-VRLLPQGTVIFEDISIEHFE
UNR_CSD3_HS DEVEFTVVPDMLSAQRNHAIR-IKKLPKGTVSFHSHSDHRFL
UNR_CSD4_HS DMVEYSL—SKGKGNKVSAEK-VNKTHSVNGITEEADPTIYS
UNR_CSD5_HS DEVEFSV-ILNQRTGKCSACN-VWRVCEGPKAVAAPRPDRLV
                 : * :.            :
```

HS:Homo Sapiens
DR:Danio Rerio
DS:Drosophila Silvestris
EC:Escherichia Coli
DM:Drosophila melanogaster

Figure 7. Sequence alignment of human YB-1 CSD with different CSDs. Numbers given on the top of the sequence are the residue numbers of human YB-1 CSD. Residues involved in ssDNA binding in our structure are boxed and labeled in red, and the conserved residues are labeled in red.

It has been reported that YB-1 binds to a variety of DNAs and RNAs including specific and non-specific substrates. The specific binding is mediated by the CSD and the non-specific binding by the CTD. Our ssDNA binding results demonstrate that YB-1 can recognize a wider range of DNA sequences than previously thought. CACC, CATC, CAAC, Y-box and CAGC motifs are all potential targets of YB-1. In addition, CACC, CAGC and CAAC are all found in RNA targets of YB-1, suggesting that YB-1 CSDex binds to similar sequences of DNAs and RNAs. Analysis of the gene promoters regulated by YB-1 reveals that they all contain one or more such motifs. For instance, MDR1 gene promoter contains CACC and CAGC, (5′-TGCCCAGCCAATCAGCCTCACCACAG-3′) (13), EGFR contains CAAC and CAGC (5′-ATGTTTA TTGCAACCAGCCATGGGTACTTTGAAGCCAA TGTGTGAA-3′) (14) and MYC gene contains CACC (5′-CCTTCCCCACCCTCCCCACCCTCCC-3′) (16). Besides ssDNAs with a CACC motif, we have observed that a dsDNA with a CACC motif binds to YB-1 CSDex more strongly than the Y-box (Supplementary Figure S8). This indicates CACC would be a more potential target of YB-1 than Y-box. Apart from the core motif, the context sequence of a DNA also affects the binding affinity as shown here. This provides a guide for future search for potential targets of YB-1 CSD.

The phosphorylation of S102 plays an important role in YB-1 regulation of DNA transcription and RNA translation. But the molecular mechanism has been unclear until this study. CSDex adopts only a folded conformation, but ^{P}S102 and point mutants S102A, S102D and S102E each exist in dynamic equilibrium between folded and locally unfolded conformations. The result shows the hydroxyl group of S102 plays a critical role in stabilizing CSDex likely through hydrogen bonding. Although our NMR structure is not accurate enough to specify sidechain hydrogen bonds, the crystal structure of the zebrafish CSD/RNA complex (PDB ID: 6A6J) shows the presence of a hydrogen bond between the sidechain OH of S82 (equivalent to human YB-1 S102) and the backbone NH of S116 (equivalent to human YB-1 S136) located at the C-terminal extension. Thus, phosphorylation of S102 disrupts its hydrogen bonding with the residue in the C-terminal extension (S136), resulting in conformational changes in the regions close to S102, and in turn destabilizing the CSDex. The conformational changes are evidenced from the differential NMR spectra of the phosphorylated and non-phosphorylated CSDex (Figure 5), including residues perturbed by the phosphorylation, which are located mainly in the C-terminal extension and loop34. The structural changes make the phosphorylated form less compatible to ssDNAs than the non-phosphorylated form. Consequently, the phosphorylation

causes dramatic reduction of the affinity of YB-1 to ssD-NAs.

Our results argue that YB-1 can bind to ssDNA, dsDNA and RNA, while the phosphorylation reduces significantly its binding affinity. Consistent with this, previous studies have shown that phosphorylation of YB-1 can activate gene translation in the cytoplasm by releasing the bound mR-NAs from YB-1 (27–29). However, how phosphorylation mediates gene transcription in the nucleus is disputable. YB-1 can act as an activator to promote gene transcription or as a repressor to repress gene transcription in the nucleus (2). Previous studies found that the phosphorylation of YB1 at S102 by AKT and RSK allows it to shuttle into the nucleus, enhances its binding to the promoters of some genes, and stimulates gene transcription by an unknown mechanism (2,52). On the other hand, it was also reported that acute stimulation of YB-1 phosphorylation does not promote YB-1 nuclear translocation (25) and both phosphorylated and non-phosphorylated YB-1 can be detected in the nucleus (53). Contrary to the reports that phosphorylation of YB-1 promotes its binding to DNA, the study on mouse MSY3 (YB-3) showed that phosphorylation decreases its binding to DNA (54). MYS3 is a close family member of YB-1. MYS3 CSDex shares 94% sequence identity with human YB-1 CSDex and can be phosphorylated by AKT at the same serine residue as human YB-1. MSY3 represses myogenin transcription and forced phosphorylation of MSY3 reduces its occupancy at the myogenin promoter, leading to myogenin up-regulation. Consistently, *in vitro* MSY3 can bind strongly to DNA, while its phosphorylation by AKT reduces the binding. These results agree with our study that the binding of YB-1 CSDex to DNA is reduced by phosphorylation. Taken together, we propose that phosphorylation of YB-1 affects gene transcription conditionally. When YB-1 acts as an activator through its binding to gene promoters, phosphorylation of YB-1 will reduce the binding and decrease the transcription; when YB-1 acts as a repressor through its binding to gene promoters, the phosphorylation will release the bound DNA to stimulate the transcription. To clarify the biological function of phosphorylated YB-1 in the nucleus, further study is needed.

DATA AVAILABILITY

The NMR assignments and structure models have been deposited in BMRB (ID: 36306 and 36307) and PDB (ID: 6LMR and 6LMS).

SUPPLEMENTARY DATA

Supplementary Data are available at NAR Online.

ACKNOWLEDGEMENTS

FUNDING

REFERENCES

1. Kleene,K.C. (2018) Y-box proteins combine versatile cold shock domains and arginine-rich motifs (ARMs) for pleiotropic functions in RNA biology. *Biochem. J.*, **475**, 2769–2784.
2. Eliseeva,I.A., Kim,E.R., Guryanov,S.G., Ovchinnikov,L.P. and Lyabin,D.N. (2011) Y-box-binding protein 1 (YB-1) and its functions. *Biochemistry (Mosc.)*, **76**, 1402–1433.
3. Kuwano,M., Shibata,T., Watari,K. and Ono,M. (2019) Oncogenic Y-box binding protein-1 as an effective therapeutic target in drug-resistant cancer. *Cancer Sci.*, **110**, 1536–1543.
4. Lyons,S.M., Achorn,C., Kedersha,N.L., Anderson,P.J. and Ivanov,P. (2016) YB-1 regulates tiRNA-induced stress granule formation but not translational repression. *Nucleic. Acids. Res.*, **44**, 6949–6960.
5. Blenkiron,C., Hurley,D.G., Fitzgerald,S., Print,C.G. and Lasham,A. (2013) Links between the oncoprotein YB-1 and small non-coding RNAs in breast cancer. *PLoS One*, **8**, e80171.
6. Wu,S.L., Fu,X., Huang,J., Jia,T.T., Zong,F.Y., Mu,S.R., Zhu,H., Yan,Y., Qiu,S., Wu,Q. *et al.* (2015) Genome-wide analysis of YB-1-RNA interactions reveals a novel role of YB-1 in miRNA processing in glioblastoma multiforme. *Nucleic Acids Res.*, **43**, 8516–8528.
7. Nasrin,F., Rahman,M.A., Masuda,A., Ohe,K., Takeda,J. and Ohno,K. (2014) HnRNP C, YB-1 and hnRNP L coordinately enhance skipping of human MUSK exon 10 to generate a Wnt-insensitive MuSK isoform. *Sci. Rep.*, **4**, 6841.
8. Kretov,D.A., Clement,M.J., Lambert,G., Durand,D., Lyabin,D.N., Bollot,G., Bauvais,C., Samsonova,A., Budkina,K., Maroun,R.C. *et al.* (2019) YB-1, an abundant core mRNA-binding protein, has the capacity to form an RNA nucleoprotein filament: a structural analysis. *Nucleic. Acids. Res.*, **47**, 3127–3141.
9. Kloks,C.P., Spronk,C.A., Lasonder,E., Hoffmann,A., Vuister,G.W., Grzesiek,S. and Hilbers,C.W. (2002) The solution structure and DNA-binding properties of the cold-shock domain of the human Y-box protein YB-1. *J. Mol. Biol.*, **316**, 317–326.
10. Swamynathan,S.K., Nambiar,A. and Guntaka,R.V. (2000) Chicken Y-box proteins chk-YB-1b and chk-YB-2 repress translation by sequence-specific interaction with single-stranded RNA. *Biochem. J.*, **348 Pt 2**, 297–305.
11. Nambiar,A., Swamynathan,S.K., Kandala,J.C. and Guntaka,R.V. (1998) Characterization of the DNA-binding domain of the avian Y-box protein, chkYB-2, and mutational analysis of its single-strand binding motif in the Rous sarcoma virus enhancer. *J. Virol.*, **72**, 900–909.
12. Didier,D.K., Schiffenbauer,J., Woulfe,S.L., Zacheis,M. and Schwartz,B.D. (1988) Characterization of the cDNA encoding a protein binding to the major histocompatibility complex class II Y box. *Proc. Natl. Acad. Sci. U.S.A.*, **85**, 7322–7326.
13. Ohga,T., Uchiumi,T., Makino,Y., Koike,K., Wada,M., Kuwano,M. and Kohno,K. (1998) Direct involvement of the Y-box binding protein YB-1 in genotoxic stress-induced activation of the human multidrug resistance 1 gene. *J. Biol. Chem.*, **273**, 5997–6000.
14. Stratford,A.L., Habibi,G., Astanehe,A., Jiang,H., Hu,K., Park,E., Shadeo,A., Buys,T.P., Lam,W., Pugh,T. *et al.* (2007) Epidermal growth factor receptor (EGFR) is transcriptionally induced by the Y-box binding protein-1 (YB-1) and can be inhibited with Iressa in basal-like breast cancer, providing a potential target for therapy. *Breast Cancer Res.*, **9**, R61.
15. Zasedateleva,O.A., Krylov,A.S., Prokopenko,D.V., Skabkin,M.A., Ovchinnikov,L.P., Kolchinsky,A. and Mirzabekov,A.D. (2002) Specificity of mammalian Y-box binding protein p50 in interaction with ss and ds DNA analyzed with generic oligonucleotide microchip. *J. Mol. Biol.*, **324**, 73–87.

16. Kolluri,R., Torrey,T.A. and Kinniburgh,A.J. (1992) A CT promoter element binding protein: definition of a double-strand and a novel single-strand DNA binding motif. *Nucleic. Acids. Res.*, **20**, 111–116.

17. Dolfini,D. and Mantovani,R. (2013) Targeting the Y/CCAAT box in cancer: YB-1 (YBX1) or NF-Y? *Cell Death Differ.*, **20**, 676–685.

18. Wei,W.J., Mu,S.R., Heiner,M., Fu,X., Cao,L.J., Gong,X.F., Bindereif,A. and Hui,J. (2012) YB-1 binds to CAUC motifs and stimulates exon inclusion by enhancing the recruitment of U2AF to weak polypyrimidine tracts. *Nucleic. Acids. Res.*, **40**, 8622–8636.

19. Skabkina,O.V., Lyabin,D.N., Skabkin,M.A. and Ovchinnikov,L.P. (2005) YB-1 autoregulates translation of its own mRNA at or prior to the step of 40S ribosomal subunit joining. *Mol. Cell. Biol.*, **25**, 3317–3323.

20. Stickeler,E., Fraser,S.D., Honig,A., Chen,A.L., Berget,S.M. and Cooper,T.A. (2001) The RNA binding protein YB-1 binds A/C-rich exon enhancers and stimulates splicing of the CD44 alternative exon v4. *EMBO J.*, **20**, 3821–3830.

21. Yang,X.J., Zhu,H., Mu,S.R., Wei,W.J., Yuan,X., Wang,M., Liu,Y., Hui,J. and Huang,Y. (2019) Crystal structure of a Y-box binding protein 1 (YB-1)-RNA complex reveals key features and residues interacting with RNA. *J. Biol. Chem.*, **294**, 10998–11010.

22. Yang,Y., Wang,L., Han,X., Yang,W.L., Zhang,M., Ma,H.L., Sun,B.F., Li,A., Xia,J., Chen,J. *et al.* (2019) RNA 5-methylcytosine facilitates the maternal-to-zygotic transition by preventing maternal mRNA decay. *Mol. Cell*, **75**, 1188–1202.

23. Stratford,A.L., Fry,C.J., Desilets,C., Davies,A.H., Cho,Y.Y., Li,Y., Dong,Z., Berquin,I.M., Roux,P.P. and Dunn,S.E. (2008) Y-box binding protein-1 serine 102 is a downstream target of p90 ribosomal S6 kinase in basal-like breast cancer cells. *Breast Cancer Res.*, **10**, R99.

24. Maier,E., Attenberger,F., Tiwari,A., Lettau,K., Rebholz,S., Fehrenbacher,B., Schaller,M., Gani,C. and Toulany,M. (2019) Dual targeting of Y-box binding Protein-1 and Akt inhibits proliferation and enhances the chemosensitivity of colorectal cancer cells. *Cancers (Basel)*, **11**, 562.

25. Tiwari,A., Rebholz,S., Maier,E., DehghanHarati,M., Zips,D., Sers,C., Rodemann,H.P. and Toulany,M. (2018) Stress-induced phosphorylation of nuclear YB-1 depends on nuclear trafficking of p90 ribosomal S6 kinase. *Int. J. Mol. Sci.*, **19**, 2441.

26. Dhillon,J., Astanehe,A., Lee,C., Fotovati,A., Hu,K. and Dunn,S.E. (2010) The expression of activated Y-box binding protein-1 serine 102 mediates trastuzumab resistance in breast cancer cells by increasing CD44+ cells. *Oncogene*, **29**, 6294–6300.

27. Evdokimova,V., Ruzanov,P., Anglesio,M.S., Sorokin,A.V., Ovchinnikov,L.P., Buckley,J., Triche,T.J., Sonenberg,N. and Sorensen,P.H. (2006) Akt-mediated YB-1 phosphorylation activates translation of silent mRNA species. *Mol. Cell. Biol.*, **26**, 277–292.

28. Bader,A.G. and Vogt,P.K. (2008) Phosphorylation by Akt disables the anti-oncogenic activity of YB-1. *Oncogene*, **27**, 1179–1182.

29. Li,D., Liu,X., Zhou,J., Hu,J., Zhang,D., Liu,J., Qiao,Y. and Zhan,Q. (2017) Long noncoding RNA HULC modulates the phosphorylation of YB-1 through serving as a scaffold of extracellular signal-regulated kinase and YB-1 to enhance hepatocarcinogenesis. *Hepatology*, **65**, 1612–1627.

30. Basaki,Y., Hosoi,F., Oda,Y., Fotovati,A., Maruyama,Y., Oie,S., Ono,M., Izumi,H., Kohno,K., Sakai,K. *et al.* (2007) Akt-dependent nuclear localization of Y-box-binding protein 1 in acquisition of malignant characteristics by human ovarian cancer cells. *Oncogene*, **26**, 2736–2746.

31. Yang,D., Zheng,Y., Liu,D. and Wyss,D.F. (2004) Sequence-specific assignments of methyl groups in high-molecular weight proteins. *J. Am. Chem. Soc.*, **126**, 3710–3711.

32. Xu,Y., Long,D. and Yang,D. (2007) Rapid data collection for protein structure determination by NMR spectroscopy. *J. Am. Chem. Soc.*, **129**, 7722–7723.

33. Ogura,K., Terasawa,H. and Inagaki,F. (1996) An improved double-tuned and isotope-filtered pulse scheme based on a pulsed field gradient and a wide-band inversion shaped pulse. *J. Biomol. NMR*, **8**, 492–498.

34. Delaglio,F., Grzesiek,S., Vuister,G.W., Zhu,G., Pfeifer,J. and Bax,A. (1995) NMRPipe: a multidimensional spectral processing system based on UNIX pipes. *J. Biomol. NMR*, **6**, 277–293.

35. Lee,W., Tonelli,M. and Markley,J.L. (2015) NMRFAM-SPARKY: enhanced software for biomolecular NMR spectroscopy. *Bioinformatics*, **31**, 1325–1327.

36. Xu,Y., Zheng,Y., Fan,J.S. and Yang,D. (2006) A new strategy for structure determination of large proteins in solution without deuteration. *Nat. Methods*, **3**, 931–937.

37. Lin,Z., Xu,Y.Q., Yang,S. and Yang,D. (2006) Sequence-specific assignment of aromatic resonances of uniformly C-13,N-15-labeled proteins by using C-13- and N-15-edited NOESY spectra. *Angew. Chem. Int. Ed. Engl.*, **45**, 1960–1963.

38. Zwahlen,C., Legault,P., Vincent,S.J.F., Greenblatt,J., Konrat,R. and Kay,L.E. (1997) Methods for measurement of intermolecular noes by multinuclear NMR spectroscopy: Application to a bacteriophage lambda n-peptide/Boxb RNA complex. *J. Am. Chem. Soc.*, **119**, 6711–6721.

39. Shen,Y., Delaglio,F., Cornilescu,G. and Bax,A. (2009) TALOS+: a hybrid method for predicting protein backbone torsion angles from NMR chemical shifts. *J. Biomol. NMR*, **44**, 213–223.

40. Brunger,A.T., Adams,P.D., Clore,G.M., DeLano,W.L., Gros,P., Grosse-Kunstleve,R.W., Jiang,J.S., Kuszewski,J., Nilges,M., Pannu,N.S. *et al.* (1998) Crystallography & NMR system: a new software suite for macromolecular structure determination. *Acta Crystallogr. D. Biol. Crystallogr.*, **54**, 905–921.

41. Schwieters,C.D., Kuszewski,J.J. and Clore,G. M. (2006) Using Xplor-NIH for NMR molecular structure determination. *Prog. Nucl. Magn. Reson. Spectrosc.*, **48**, 47–62.

42. Bermejo,G.A., Clore,G. M. and Schwieters,C.D. (2016) Improving NMR structures of RNA. *Structure*, **24**, 806–815.

43. Tian,Y., Schwieters,C.D., Opella,S.J. and Marassi,F.M. (2014) A practical implicit solvent potential for NMR structure calculation. *J. Magn. Res.*, **243**, 54–64.

44. Fan,J.S., Goh,H., Ding,K., Xue,B., Robinson,R.C. and Yang,D. (2017) Structural basis for pH-mediated regulation of F-actin severing by gelsolin domain 1. *Sci. Rep.*, **7**, 45230.

45. Kloks,C.P., Tessari,M., Vuister,G.W. and Hilbers,C.W. (2004) Cold shock domain of the human Y-box protein YB-1. Backbone dynamics and equilibrium between the native state and a partially unfolded state. *Biochemistry*, **43**, 10237–10246.

46. Hou,H., Wang,F., Zhang,W., Wang,D., Li,X., Bartlam,M., Yao,X. and Rao,Z. (2011) Structure-functional analyses of CRHSP-24 plasticity and dynamics in oxidative stress response. *J. Biol. Chem.*, **286**, 9623–9635.

47. Nam,Y., Chen,C., Gregory,R.I., Chou,J.J. and Sliz,P. (2011) Molecular basis for interaction of let-7 microRNAs with Lin28. *Cell*, **147**, 1080–1091.

48. Hennig,J., Militti,C., Popowicz,G.M., Wang,I., Sonntag,M., Geerlof,A., Gabel,F., Gebauer,F. and Sattler,M. (2014) Structural basis for the assembly of the Sxl-Unr translation regulatory complex. *Nature*, **515**, 287–290.

49. Goroncy,A.K., Koshiba,S., Tochio,N., Tomizawa,T., Inoue,M., Watanabe,S., Harada,T., Tanaka,A., Ohara,O., Kigawa,T. *et al.* (2010) The NMR solution structures of the five constituent cold-shock domains (CSD) of the human UNR (upstream of N-ras) protein. *J. Struct. Funct. Genomics*, **11**, 181–188.

50. Schindelin,H., Jiang,W., Inouye,M. and Heinemann,U. (1994) Crystal structure of CspA, the major cold shock protein of Escherichia coli. *Proc. Natl. Acad. Sci. U.S.A.*, **91**, 5119–5123.

51. Mayr,F., Schutz,A., Doge,N. and Heinemann,U. (2012) The Lin28 cold-shock domain remodels pre-let-7 microRNA. *Nucleic Acids Res.*, **40**, 7492–7506.

52. Astanehe,A., Finkbeiner,M.R., Hojabrpour,P., To,K., Fotovati,A., Shadeo,A., Stratford,A.L., Lam,W.L., Berquin,I.M., Duronio,V. *et al.* (2009) The transcriptional induction of PIK3CA in tumor cells is dependent on the oncoprotein Y-box binding protein-1. *Oncogene*, **28**, 2406–2418.

53. Sinnberg,T., Sauer,B., Holm,P., Spangler,B., Kuphal,S., Bosserhoff,A. and Schittek,B. (2012) MAPK and PI3K/AKT mediated YB-1 activation promotes melanoma cell proliferation which is counteracted by an autoregulatory loop. *Exp. Dermatol.*, **21**, 265–270.

54. De Angelis,L., Balasubramanian,S. and Berghella,L. (2015) Akt-mediated phosphorylation controls the activity of the Y-box protein MSY3 in skeletal muscle. *Skelet Muscle*, **5**, 18.